



# An explainable deep learning framework for accurate and automated cardiac arrhythmia classification using Electrocardiogram signals

P. Kavitha<sup>\*</sup>, L. Shakkeera

School of Computer Science and Engineering, Presidency University, Bengaluru, Karnataka 560064, India

## ARTICLE INFO

**Keywords:**  
 Electrocardiogram  
 Denoising  
 Feature extraction  
 Arrhythmia  
 Explainable AI  
 Deep learning

## ABSTRACT

Cardiac arrhythmias, a significant subcategory of cardiovascular diseases (CVDs), are known to have severe implications for patient health. Given that certain cardiac conditions induce sudden cardiac arrest, Electrocardiogram (ECG) signals provide critical diagnostic information for identifying these anomalies. However, accurately classifying arrhythmic patterns is challenging due to ECG signals including low amplitude, short duration, high variability among patients, and overlapping waveform features. This research proposes an explainable deep learning architecture for accurate and automated detection of cardiac arrhythmias based on ECG signals to address these challenges. The proposed model, that is cycle-consistent convolutional momentum colour harmony after-image generative adversarial network, employs sophisticated feature extraction and generative learning methods for precision arrhythmia classification. It preprocesses according to the steps consisting of denoising, peak detection, segmentation and temporal feature extraction to evaluate the probability of each category of arrhythmia and choose one with the maximum probability as its final prediction. Other improvements to the convergence speed and segmentation accuracy include the incorporation of the artificial after-image algorithm and colour harmony, which capability a robust hyperparameter optimization. Shapley additive explanations to ensure the model's interpretability, which show prominent features affecting its decision-making, as well as enhancing clinician trust in the system. The outcomes determine that the proposed framework attains remarkable accuracy across datasets: 99.87% on the MIT-BIH Arrhythmia Dataset, 99.88% on the MIT-BIH Supraventricular Arrhythmia dataset, 99.88% on the 12-lead ECG dataset and 99.88% on the PTB-XL ECG. It ensures rapid diagnosis, high reliability, and interpretability of cardiac arrhythmias.

## 1. Introduction

The CVDs are worldwide known as the major cause of death [1]. Out of all the manifestations, myocardial infarction and cardiac arrhythmias, irregular heart rhythms are particularly diagnostic challenges because of its potentially abrupt and fatal nature. ECG captures the heart's cyclical contractions and relaxations, typically represented through waves such as the P wave, QRS complex, and T wave [2–4]. Interpretation of these ECG signals forms the foundation for diagnosing arrhythmias. However, arrhythmias are often paroxysmal and transient, making it difficult to detect reliably during brief monitoring periods. Traditionally, arrhythmia detection methods have used signal denoising [5–8], waveform segmentation, and manual extraction of features. However, these approaches often suffer from limitations: noise sensitivity, considerable variability in ECG morphology between patients, and, typically, a narrow focus on isolated cycles that neglect longer patterns

in the temporal axes. One of the main difficulties is the correct detection of the QRS complex, duration, amplitude, and types of arrhythmias. Moreover, motion artefact and baseline drift make detection even less reliable [8]. Fig. 1 illustrates the fiducial points within an electrocardiogram (ECG) and the features of the ECG waveform that serve as key markers when it comes to the analysis of heart rhythms, rate, and abnormalities.

One of the consequences of this challenge is the efficient application of Deep Learning (DL) technologies for automatic arrhythmia classification using the ECG signal. Consisting of multiple nonlinear layers, DL models automatically learn hierarchical features from raw ECG signals, providing a scalable means of cardiac rhythm analysis with accuracy. Nevertheless, to achieve the highest performance with different ECG datasets, much more robust and interpretable solutions are still needed to address these challenges. This research proposed an explainable DL-based method. The examination consists of denoising to get clear of

\* Corresponding author.

E-mail addresses: [kavitha.2023cse0024@presidencyuniversity.in](mailto:kavitha.2023cse0024@presidencyuniversity.in) (P. Kavitha), [shakkeera.l@presidencyuniversity.in](mailto:shakkeera.l@presidencyuniversity.in) (L. Shakkeera).

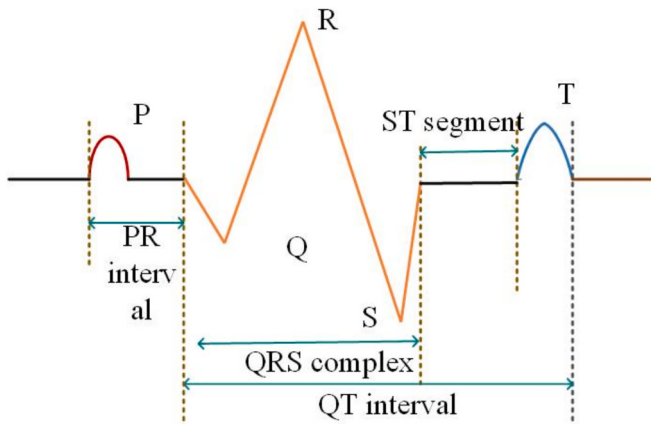


**Fig. 1.** Key landmarks and characteristics of the ECG signal.

baseline drift and powerline noise, peak detection for P, R, T waves, splitting into single beats, and temporal feature extraction to keep inter-beat variability.

The major contributions of the research include.

- By imposing cycle consistency, the model prevents mapping an arrhythmic ECG to a normal one and then back to the original input. This regularization supports morphological traces for enhancing and maintaining temporal coherence in ECG analysis.
- The generator of the Generative Adversarial Network (GAN) synthesizes rare or underrepresented arrhythmia classes, and it helps mitigate class imbalance as well as detect clinically relevant arrhythmias.
- Utilized Shapley Additive Explanations (SHAP) to identify dominant temporal-spatial factors with minimal reliance on subject-specific metadata. Maintained high generalizability and low computational burden.

The remainder of this research is structured as follows: In [Section 2](#), related works on ECG-based arrhythmia detection and classification are discussed. [Section 3](#) elaborates on the proposed framework and its main components. Experimental setup, evaluation metrics, and comparative results are explained in [Section 4](#). The conclusion and future study directions are laid out in [Section 5](#).

## 2. Related works

### 2.1. Deep Learning-Based ECG arrhythmia classification methods

In 2025, Lamba et al. [9] presented a Feature extraction and Arrhythmia classification using DL from ECG signals (FADLEC). Outstanding performance at 99.1% multi-class arrhythmia detection, and are used for capturing both temporal and frequency-domain ECG features. Although Ant Colony Optimization (ACO) and DL training are computationally costly, particularly for big data or real-time scenarios. In 2022, Bhatia et al. [10] suggested a CNN and BiLSTM for ECG signal segmentation, achieving an accuracy of 98.36%. Applies CNN's spatial extraction alongside Bi-LSTM's sequential learning for enhanced feature representation. However, no preprocessing or filtering component is present for signal quality estimation or denoising. In 2024, Eleyan et al. [11] suggested an LSTM and a CNN for the classification of ECG signals. CNN captures morphological characteristics (e.g., QRS complex morphology), and LSTM learns time-series relationships (e.g., heartbeat patterns). The model exhibited excellent performance in discriminating arrhythmia classes. Whereas the model is tested primarily on pre-recorded datasets, performance on real-time or multiple-lead ECG signals is not investigated. State-of-the-art attention-based models (e.g.,

Transformers) for time series were not compared to the CNN-LSTM hybrid. In 2025, Lim et al. [12] suggested adaptive DL techniques with beat segmentation and relative heart rate integration for ECG analysis. Overcomes the limitations of fixed-duration segmentation by dynamically adapting to RR intervals to minimize segmentation errors. Incorporates relative heart rate data that improves detection accuracy, especially for arrhythmic beats. In 2024, Kim et al. [13] suggested a residual CNN and Global Channel Attention Block (GCAB) for the classification of multi-label cardiac arrhythmia. Efficiently classifies 45 various cardiac arrhythmias, hence being among the most comprehensive classifiers used in ECG processing. The GCAB enables the method to concentrate on the high-signal channels and features of the signal, improving accuracy for difficult arrhythmias. The attention mechanisms increase focus, but the model itself is still a black-box and therefore doesn't increase clinical interpretability. In 2025, Guerra et al. [14] recommended an autoencoder-enhanced LSTM-based multi-class classifier for ECG arrhythmia detection. Denoising and dimensionality reduction networks fit well with data like ECG for time series applications for the detection of temporal patterns, which are pertinent to recognition of the type of arrhythmia. However, the combination of an autoencoder and LSTM creates a black-box model that does not favour interpretability. In 2022, Rahman et al. [15] suggested a Transfer Learning (TL) model for ECG arrhythmia detection and classification. The model makes training faster and uses rich general features from large amounts of data. Perhaps able to detect multiple arrhythmia classes rather than binary classification. TL models have no explainability, which is very important in clinical applications. There are no XAI tools, such as SHAP or LIME, implemented.

### 2.2. Gan-based approaches for ECG

In 2023, Xia et al. [16] suggested a GAN generator based on the Transformer framework to augment the morphology of ECG and improve the classification downstream. Such a scheme is shown to augment feature diversity by combining GAN-based augmentation and self-attention. However, transformer generators require high computational resources and do not have mechanisms that enforce physiological consistency during reconstruction. In 2025, Zarean et al. [17] suggested an attention-based CNN-LSTM model that is resistant to GAN-generated adversarial EEG signals for biometric identification. Even if it successfully learning sequence-dependent features, this model focuses on adversarial robustness and not morphology enhancement, which then limits its direct applicability to ECG pathology classification. In 2025, Haseena et al. [18] suggested a GAN-driven feature selection strategy combined with a hybrid DL classifier for heartbeat recognition. Illustrated that GAN-enhanced feature refinement significantly raised class separability. Thus, the ability to reconstruct physiologically meaningful signals or correct generative distortions is limited.

In 2023, Qin et al. [19] suggested a Multi-View Knowledge Transfer ECG (MVKTECG) for single-lead ECG diagnosis. Enables a single-lead ECG to take advantage of more detailed monitoring from a multi-lead ECG, enhancing performance without added input complexity. It can be used to diagnose multiple cardiac diseases at a time, which is essential in clinical practice. Whereas this interaction of these methods adds training overhead, which is not always possible to accommodate in real-time embedded systems. In 2022, Ullah et al. [20] introduced a 2D CNN-based DenseNet model for automatic ECG arrhythmia recognition. Reached 99.50% accuracy, 98.91% F1-score, and 98.94% precision, which outperforms several other models present. The DenseNet structure facilitates better gradient flow and feature reuse, resulting in quicker convergence and ultimately better performance. Usage of the DenseNet with 2D CNNs requires a lot of processing power, which presents a difficulty for edge or wearable gadgets. In 2024, Xu et al. [21] developed a Multi-Modality Data Augmentation Network (MM-DANet). By fusing rich representations of signals, MM-DANet extracts complementary information from modalities and enhances accuracy. Multiview

**Table 1**  
Summary of related works.

Author	Method	Advantages	Disadvantages
Lamba et al. [9]	FADLEC	Combining SW-HT and deep learning achieves 99.1% multi-class accuracy.	High computational cost due to ACO and DL training.
Rahman et al. [15]	TL	Reduces training time, leverages pretrained models for multi-class detection.	Lacks XAI tools for clinical interpretability.
Bhatia et al. [10]	CNN-BiLSTM	Captures spatial and sequential features, achieves 98.36% accuracy.	No preprocessing for signal quality improvement.
Eleyan et al. [11]	CNN-LSTM	Combines CNN and LSTM for feature extraction from ECGs; tested on MIT-BIH and BIDMC datasets.	Lacks transformer comparison.
Lim et al. [12]	Adaptive DL with RR Interval Segmentation	Dynamic segmentation minimizes errors.	Real-time streaming performance is not addressed
Kim et al. [13]	Residual CNN with GCAB	Efficiently classifies 45 arrhythmia types, enhances focus using attention mechanisms.	The model remains a black-box, limiting interpretability.
Qin et al. [19]	MVKTECG	Multi-view knowledge transfer improves single-lead ECG diagnosis.	Training overhead hinders real-time deployment.
Ullah et al. [20]	2D CNN-Based DenseNet	Achieves 99% accuracy, improved gradient flow, and feature reuse.	High computational cost for the edge.
Xu et al. [21]	MM-DANet	Multimodal ECG fusion enhances robustness and accuracy.	Generalization to unseen pathologies is not explored.
Guerra et al. [14]	Autoencoder-Enhanced LSTM	Denoising and dimensionality reduction improve temporal feature extraction.	The black-box nature limits clinical interpretability.

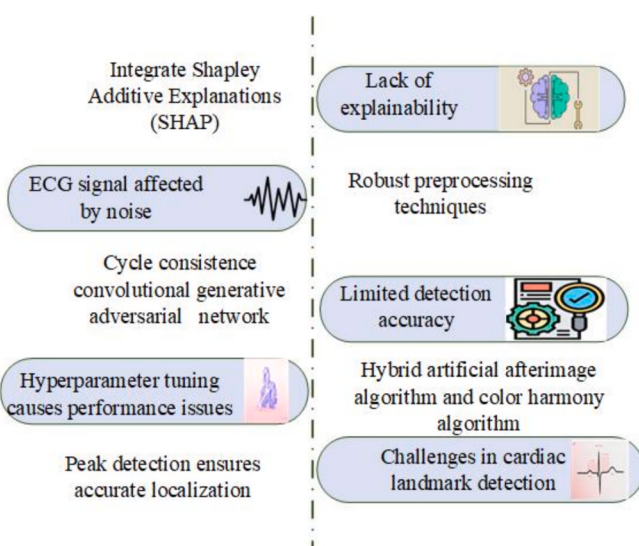


Fig. 2. Research gap and solution of the proposed method.

ECG augmentation increases robustness and facilitates distinguishing many types of arrhythmia method was optimized for arrhythmias encountered in training; generalization to unknown pathologies was not explored. Table 1 provides a summary of the existing methods for ECG classification.

### 2.3 Research gap and solution

Fig. 2 depicts one of the most critical spaces in ECG analysis research, with regard to the absence of explainability, noise disturbance, imprecision in recognition, and the requirement for hyperparameter tuning. These problems are solved by the proposed method with the help of SHAP incorporation for explainability, robust preprocessing, hybrid algorithms for accuracy, and, of course, the effective peak detection of cardiac landmark localization.

### 3. Proposed method for arrhythmia classification using Electrocardiogram signals

The ECG signal is obtained from the datasets with a preprocessing method on the ECG signals. This research proposes a new DL architecture, Cycle-Consistent Convolutional Momentum Colour Harmony Afterimage- GAN (Cycle-CMCHA-GAN), for robust cardiac arrhythmia classification. By means of sophisticated feature extraction and generative learning methods, the system permits a diagnosis that is both spatial and completely automated. The classification accuracy and convergence speed are improved by the use of the Artificial Afterimage (AA) and Colour Harmony (CH) techniques. Also, interpretability is enhanced using SHAP, which facilitates open decision-making through the identification of major risk factors, model output explanation, and enhanced clinician confidence in the diagnostic reliability of the system. Fig. 3 illustrates the overall working process of the proposed method.

#### 3.1. Data collection and Pre-Processing of ECG signal

ECG signals are gathered from four major datasets MIT-BIH dataset, the 12-lead ECG, the MIT-BIH Supra-ventricular Arrhythmia, PTB-XL ECG Datasets to ensure diverse samples for arrhythmia classification.

##### 3.1.1. Dataset Descriptions

**(a) MIT-BIH dataset [9]:** It consists of 48 recordings of ECG signals obtained from 47 individual subjects. Each record is a 30-minute excerpt from a 24-hour recording session. Table 2 shows the patient split of the datasets.

**(b) 12-lead ECG dataset [13]:** A large 12-lead ECG dataset compiled based on information from 13,241 ECG tests performed at Konkuk University Hospital in South Korea. ECG lead, as explained in Table 3.

**(c) MIT-BIH Supra-ventricular Arrhythmia [21]:** It comprises 78 two-lead ECG recordings, 30 min in duration, and sampled at 128 Hz. According to the Association for the Advancement of Medical Instrumentation (AAMI) standards, the dataset is suitable for model evaluation.

**(d) PTB-XL ECG Dataset [22]:** It is a large 12-lead ECG dataset with 21,837 recordings annotated by cardiologists, including 71 diagnostic classes such as arrhythmias, conduction blocks, myocardial infarction, hypertrophy, and ST-T abnormalities.

##### 3.1.2. Preprocessing

The unprocessed ECG signal  $s$  is fed through an organized pre-processing pipeline designed for noise reduction and significant feature extraction:

**Denoising:** A notch filter is initially applied to eliminate powerline noise at 50 Hz and 60 Hz. To further purify the signal, Discrete Wavelet Transform (DWT) is employed to reject zero wander and muscle noise, with only diagnostically important parts being retained.

**R-Peak Detection & Beat Segmentation:** On the denoised signal  $n$  R-peaks are correctly identified to act as anchor points. The signal is segmented into individual ECG beats around each R-peak. These segmental 'beats' then become a fundamental unit of analysis in processing.

**Temporal Feature Extraction:** Extraction of temporal features is conducted per beat in the ECG signal in order to detect changing patterns or temporal variability [23]. These are: RR intervals, QRS duration, QT intervals, ST segment duration, and heartbeat regularity

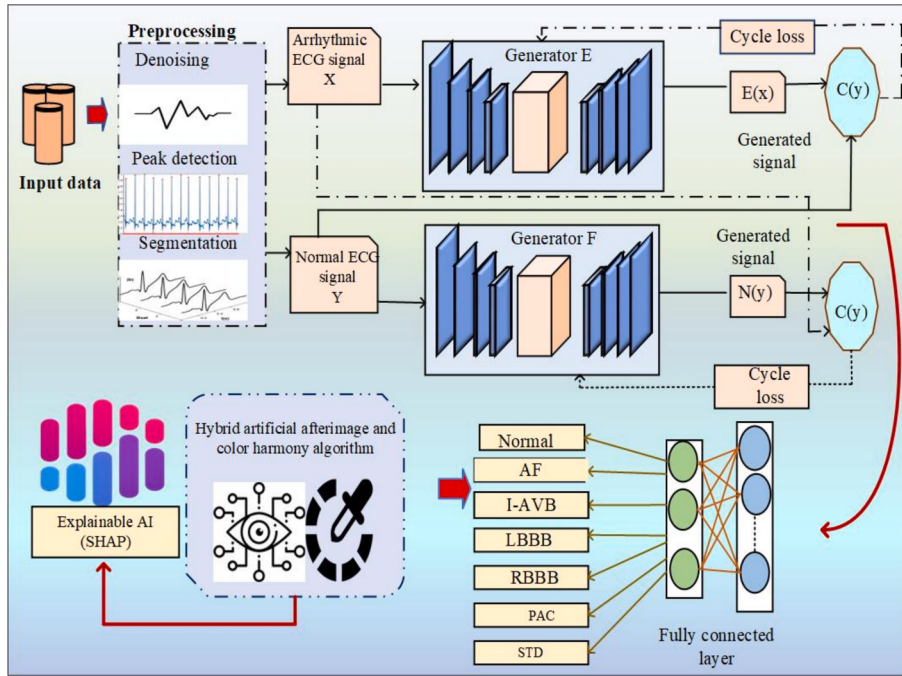


**Fig. 3.** Overall architecture of the proposed method.

**Table 2**  
MIT-BIH Arrhythmia patient splits.

Datasets	Patient IDs included
DS1 Training (DS11)	101, 106, 108, 109, 114, 115, 116, 119, 122, 209, 223
DS1 Validation (DS12)	112, 118, 124, 201, 203, 205, 207, 208, 215, 220, 230
DS2 Testing	100, 103, 105, 111, 113, 117, 121, 123, 200, 202, 210, 212, 213, 214, 219, 221, 222, 228, 231, 232, 233, 234

measures. These timestamps assist in identifying a rhythm-related abnormality. Moreover, further enhance the morphological descriptors learned from the DL model.

**Dataset Partitioning and Class Analysis:** After preprocessing, the feature-augmented beats are divided following the DS1/DS2 protocol. DS11 is used for training, DS12 is used for validation, and DS2 is used for testing. Inter-patient data partitions were, thus, meticulously maintained. Among all, the class imbalance in dataset DS1 was studied. For each class, the proportion of samples in the training set is calculated in Equation (1).

**Table 3**  
Mapping of Index Values to Corresponding ECG Leads.

Index	1	2	3	4	5	6	7	8	9	10	11	12
Lead	I	II	III	aVR	aVL	aVF	V1	V2	V3	V4	V5	V6

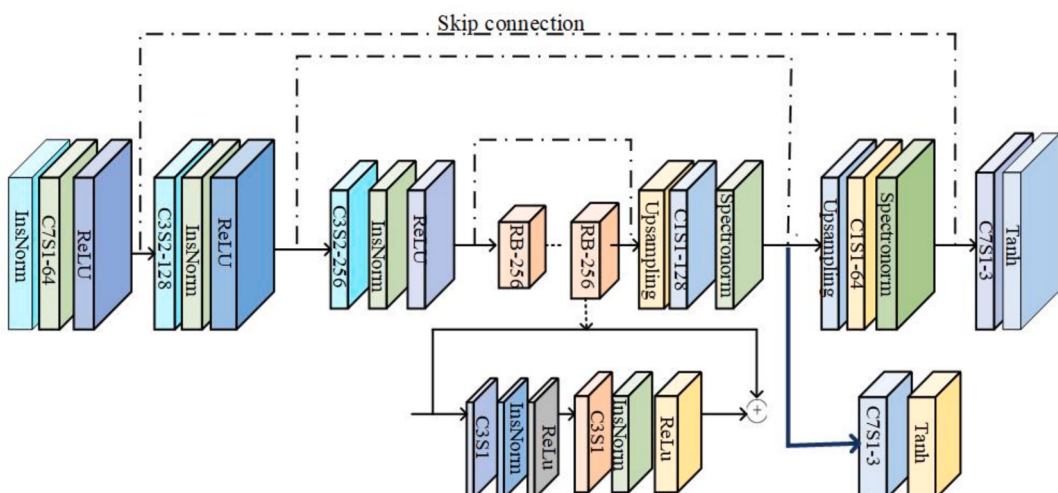


**Fig. 4.** Architecture of the generator.

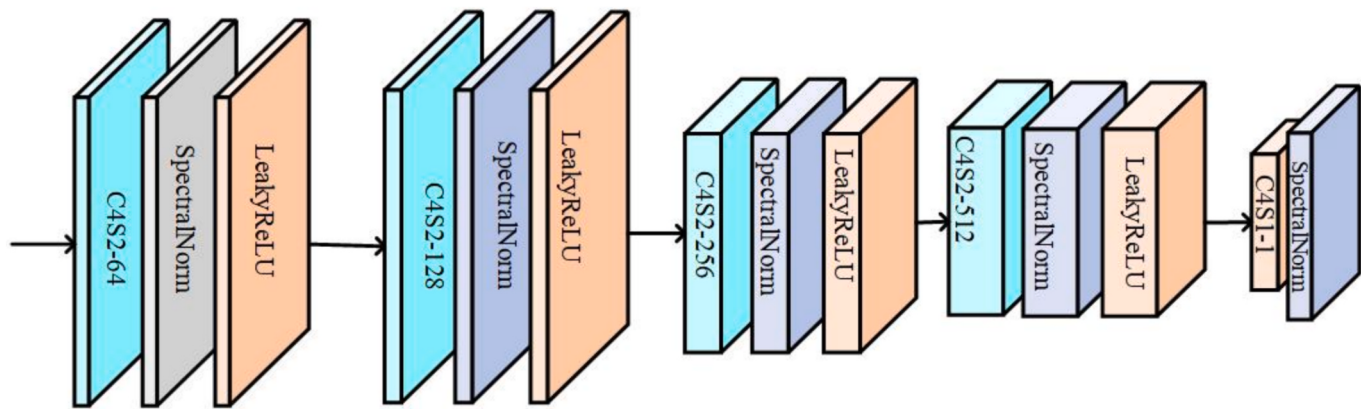


Fig. 5. Architecture of the discriminator.

**Table 4**  
Layer-wise Details and Parameters of the proposed method.

Module	Layers	Output Shape	Activation	Params
Generator	Conv1 (7 × 1, 64)	256 × 64	ReLU	512
	Conv2 (5 × 1, 128)	256 × 128	ReLU	41,088
	Conv2 (5 × 1, 128)	128 × 128	ReLU	98,560
		128		
		256		
	2 × Residual Blocks	128 × 256	ReLU	262,656
Discriminators	Momentum Conv Block	128 × 256	ReLU	98,560
	Upsample + Decoder	256 × 128	ReLU	32,896
	Output Conv	256 × 1	Tanh	129
	Conv (64, 128, 256, 512, 1)	32 × 1	Leaky ReLU/ sigmoid	690,00
Classifier	Conv1 (7 × 1, 64)	256 × 64	ReLU	512
	Conv2 (5 × 1, 128)	256 × 128	ReLU	41,088
	Feature Projection (Dense 512, 128 × 256)	128 × 256	ReLU	98,560
	Output Layer (N classes)	N	Softmax	(128 × N) + N

$$T_i = \frac{M_j}{M} \quad (1)$$

where  $M_j$  is the number of samples in class  $c_i$  and  $M$  total count of training samples presents in DS1. The majority classes are labeled as majority ( $C_{maj}$ ) and minority ( $C_{min}$ ) based on a predefined threshold. A predefined threshold  $TH$  are given in Equations (2) and (3).

If  $T_j > TH \Rightarrow C_{maj} \leftarrow C_j$  (majority class) (2).

If  $T_i < TH \Rightarrow C_{min} \leftarrow C_i$  (minority class) (3).

To deal with class imbalance, the mentioned strategies are applied:

(a) **Oversampling of Minority Classes:** The application of the SMOTE technique on the minority classes of DS1 helps in increasing the representation of these classes.

(b) **Class Weighting in Loss Function:** To ensure the model puts the right amount of emphasis on the minority classes, class weighting is also applied during training. The class weights are computed as in Equation (4).

$$\text{class\_weight}_c = \frac{N_{total}}{N_{class}} \quad (4)$$

where  $N_{class}$  is the number of samples in class  $c$  and  $N_{total}$  is the number of training samples. The method of weighting contributed to the

model learning more efficiently from the minority classes, thus providing a better performance over all arrhythmia types. The techniques for class imbalance are applied, and prepared ECG beats, like noise removal, normalization, segmentation, feature extraction, and the balanced dataset were then introduced into the Cycle-CMCHA-GAN framework for arrhythmia classification.

### 3.2. Cycle-Consistent convolutional momentum color harmony afterimage generative adversarial network for classification of cardiac arrhythmias

The model features have two bidirectional translation cycles: (1) arrhythmic normal arrhythmic cycle (forward path), (2) normal arrhythmic normal cycle (backward path). Let the arrhythmic ECG space is represented as  $Y = \{y^i\}$ , where  $y \in Y$ , and the normal ECG space is represented as  $X = \{x^i\}$ , where  $x \in X$ . That these spaces are unpaired, there is no one-to-one relationship between  $y^i$  and  $x^i$ . Forward translation cycle of the generator  $E$  translates arrhythmic ECG signals  $y \in Y$  into the normal space  $E(y) \rightarrow \hat{x} \in X$ , replicating the normal ECG signal's morphology. Generator  $N$  then tries to reconstruct the original arrhythmic signal from the generated normal one:  $N(E(y)) \rightarrow \hat{y} \approx y$ , ensuring cycle consistency and semantic accuracy. Backward Translation Cycle: The generator  $N$  translates normal ECG signals  $x \in X$  into the arrhythmic space:  $N(x) \rightarrow \hat{y} \in Y$ . Generator  $E$  then tries to rebuild the initial normal signal:  $E(N(x)) \rightarrow \bar{x} \approx x$  finishing the reverse transformation cycle [24]. Every generator in Cycle-CMCHA-GAN generates two outputs- one at the native scale and another at a detailed, higher-level semantic scale. These are processed by two matching discriminators per domain, which check temporal-spatial consistency and signal genuineness at several scales. This confrontation at multiple scales enhances the ECG generation and reconstruction process, sharpening nuanced morphological differences that are vital for arrhythmia classification.

#### Generator.

The generator utilizes a momentum-augmented encoder-decoder model with skip connections to maintain great resolution ECG features. It comprises multi-scale encoding, a residual feature transformation block, and an interpolation-based decoder combined with spectral normalization. This architecture facilitates successful translation between arrhythmic and normal ECG signals with signal integrity and classification accuracy. Fig. 4 illustrates the structure of the generator.

To improve gradient propagation and capture deep temporal dynamics, each generator produces two outputs: One from the final layer ( $x'_1, y'_1$ ) capturing global morphology; One from a hidden layer ( $x'_2, y'_2$ ) emphasizing intermediate-level transformations. Introduce dual discriminators per domain:  $C_1^X, C_2^X$  for the normal ECG domain and  $C_1^Y, C_2^Y$  for the arrhythmic ECG space. In order to enforce multi-resolution adversarial consistency, the discriminators evaluate the two output

**Table 5**

Algorithm of the hybrid artificial afterimage algorithm and color harmony algorithm.

```

1.Begin
2.Initialize parameter: max iterations ( $I_{\max}$ ), population size ( $S$ ), number of decision variables ( $V$ ), color bounds: $Colr\_lwr[b], colr\_upr[b]$ 
3. Initialize color harmony population:
For each individual  $b \in [1, S]$ 
for each dimension  $r \in [1, V]$ 
 $rdm \leftarrow rand() \in [0, 1]$ 
 $colr_{b,r} = colr_{lwr}[b] + rand() \times (colr_{upr}[b] - colr_{lwr}[b])$ 
4. Set initial AAIA population: $pop[i][j] \leftarrow colr[p][q]$ 
5. Initialize:
 $best[1][j] \leftarrow argmin(loss(pop[j][i]))$ 
 $worst[j][i] \leftarrow argmax(loss(pop[j][i]))$ 
6.  $count \leftarrow 0$ 
7. while ( $count \leq I_{\max}$ ) do
For each individual  $j \in [1, S]$ 
For each dimension  $i \in [1, V]$ 
//step1: calculate visual angle
 $P = 2 \cdot \tan^{-1} \left( \frac{pop[i][j]}{2 \cdot (pop[j][i] - best[1][i])} \right)$ 
//step2: calculate afterimage
 $N = P \cdot (pop[j][i] - best[1][i])$ 
//step 3: color harmony correction
If violates color harmony ( $N$ ) then
 $N = HarmonyCorrect(S)$ 
End if//Step 4: update candidate position
(perception-guided)
 $pop[j][i] = N + (N - best[1][i] - (worst[j][i] - pop[j][i])) \cdot ran()$ 
End for
End for
//Step5: fitness evaluation
For each individual  $j$ 
 $fitness[j] \leftarrow \alpha \times (1 - segmentation\_error[j]) +$ 
 $\beta \times color\_contrast\_score[j] +$ 
 $\gamma \times SSIM\_score[j]$ 
end for
//step 6: update global bestIf fitness
(local best) < fitness(global_best), then
Best  $\leftarrow localbest$ 
End if
 $count \leftarrow count + 1$ 
end while
8. output:best[1][j](optimal classification result)
9. end

```

**Table 6**

Hyperparameter value of the proposed method.

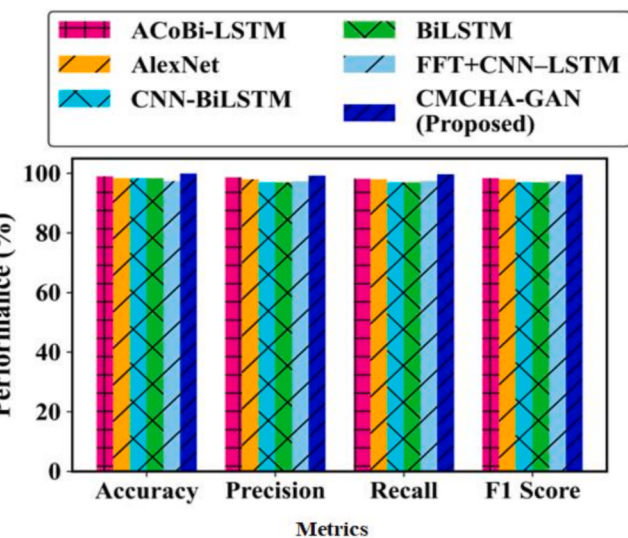
Hyperparameters	Values
Optimizer	Artificial afterimage
Learning rate	0.001
Batch size	64
Number of epochs	150
Loss function	Cross-Entropy + Cycle Consistency Loss
Activation Functions	ReLU, Softmax
Momentum	0.9
Weight Decay	1e-4
Learning Rate Decay	Exponential decay (0.96)
Early Stopping	Patience = 10 epochs

levels against each other. This process contributes to the reduction of gradient vanishing and the improvement of output quality. Let  $Y = \{y_j\}$  denote the gathering of arrhythmic ECG signals and  $X = \{x_j\}$ . The collection of normal ECG signals (unpaired, i.e.,  $j \neq i$ ). Forward Translation is given in Equations (5) and (6).

$$x'_1, x'_2 = E(y)_1, E(y)_2 \quad (5)$$

$$y'_1, y'_2 = E(x)_1, E(x)_2 \quad (6)$$

where  $E(y)_1$  and  $E(y)_2$  represent outputs from the final and hidden layers of the generator  $E$ , respectively.  $N(x'_1)$  and  $N(x'_2)$  represent reconstructions from the generator  $N$ . Discriminators  $C_1^X$  and  $C_2^X$  are used to

**Fig. 6.** Performance comparison on the MIT-BIH dataset.**Table 7**

Class-wise performance metrics on the mit-bih dataset.

Class	Precision (%)	Recall (%)	F1-Score (%)	MCC	Balanced accuracy (%)
Normal	98.5	99.2	98.8	0.96	98.9
Ventricular	89.5	87.1	88.3	0.85	88.2
Supraventricular	92.3	91.5	91.9	0.89	92.1
Fusion	85.3	82.7	83.8	0.80	83.2
Unknown	80.3	75.3	77.6	0.75	76.2

guide  $x'_1$  and  $x'_2$ . Backward Translation is given in Equations (7) and (8).

$$y''_1, y''_2 = N(x)_1, N(x)_2 \quad (7)$$

$$x''_1, y''_2 = E(y''_1)_1, E(y''_2)_2 \quad (8)$$

where  $N(x)_1$  and  $N(x)_2$  denotes the arrhythmic signal approximations from normal ECGs and  $E(y''_1)_1, E(y''_2)_2$  denotes the reconstructions back to the normal domain. Discriminators  $C_1^Y$  and  $C_2^Y$  regulate the quality of the reconstructed arrhythmic signals and regularize the training process.

#### Discriminator.

The Cycle-CMCHA-GAN uses two discriminators to separate true and synthetic ECG signals, which regulate the generator toward higher-quality outputs. The two-scale detection mechanism identifies global rhythms and local aberrations simultaneously, reduces gradient errors, and eventually makes convergence more stable, which leads to the classification of arrhythmias with higher accuracy, in comparison to single-discriminator setups. Fig. 5 illustrates the architecture discriminator in the proposed method.

The architecture features each discriminator following a structural design similar to PatchGAN, but with alterations for the 1D ECG signal. LeakyReLU is the employed activation function, preventing learning from negative-valued signals typical of ECG sequences. The output channels for the convolutional layers are set as. The same structure is applied to  $C_1^X$  and  $C_2^X$  discriminators evaluating outputs in the normal ECG domain and  $C_1^Y$   $C_2^Y$  discriminators supervising outputs in the arrhythmic domain. Table 4 explains the architecture and Layer-wise Configuration of the Proposed Generator, Discriminator, and Classifier Networks.

#### CNN-Based Classification Head.

Following signal translation and adversarial supervision, the produced ECG representations are then fed into a CNN classification head for ultimate rhythm labelling [25].

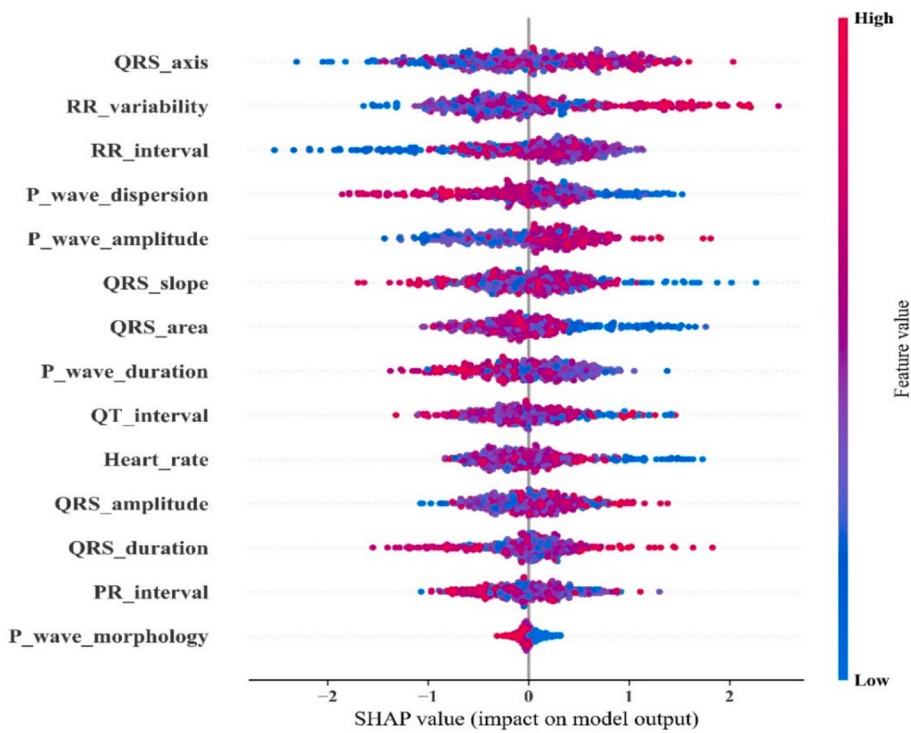


Fig. 7. SHAP summary plot.

**Table 8**  
SHAP-based ECG feature contribution on MIT-BIH dataset.

Feature	SHAP Importance Score	Interpretation
QRS complex	0.350	Strongest contributor; indicates ventricular depolarization abnormalities.
RR interval	0.290	Captures rhythm irregularity (AF, tachy/ brady patterns).
T-wave morphology	0.210	Important for repolarization changes (MI, ischemia).
P-wave characteristics	0.170	Influences supraventricular beat classification.
QT interval	0.120	Represents repolarization duration and conduction delays.
QRS Slope/Width	0.110	Highlights PVC and bundle branch block patterns.

**Table 9**  
Patient-level training and testing split with ECG beat distribution.

Dataset	Q	F	V	S	N	Total
Training (DS1)	0	512	4,980	1,965	60,880	68,337
Testing (DS12)	0	309	1,970	938	28,218	31,435
Total	0	821	6950	2903	89,098	99,772

The architecture consists of: a flattened layer – transforms the feature maps to a single 1D vector. Fully connected layer – The initial dense layer consists of 512 nodes with ReLU activation, followed by a dropout layer. Output layer: a second dense layer with SoftMax activation, having N nodes, where N = number of arrhythmia classes, outputs a class-wise probability distribution given in Equation (9).

$$O_i(\text{output}) = \frac{e^{z_i}}{\sum_{i=1}^N e^{z_i}} \quad (9)$$

where  $z_i$  specifies the outcome of the GAN and  $N$  indicates the number of classes(arrhythmia types),  $O_i$  represents the predicted probability for the class  $j$ .

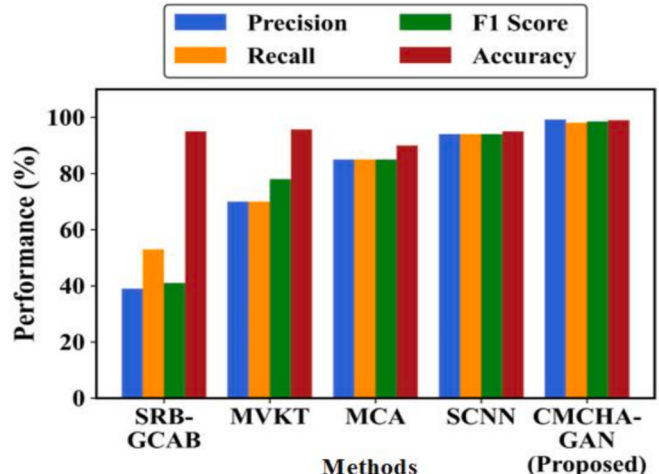


Fig. 8. Performance comparison on 12-lead ECG dataset.

#### Loss function

To provide high-fidelity ECG signal transfer and stable arrhythmia categorization, the Cycle-CMCHA-GAN supports a composite loss mechanism, fusing cycle consistency loss, dual-scale adversarial loss, and guided regularization. To ensure signal integrity and keep clinically significant temporal structures (e.g., P-QRS-T morphology) intact over domain translations, impose cycle consistency between the generator mappings  $y \rightarrow E(y)_1 \rightarrow N(E(y)_1)_1 \approx y, x \rightarrow N(x)_1 \rightarrow E(N(y)_1)_1 \approx x$

Cycle consistency loss is given in Equation (10).

$$L_c(E, N) = A_{y \sim P_{\text{data}(y)}} \|(N(E(y)_1)_1 - y)\|_1 + A_{x \sim P_{\text{data}(x)}} \|(E(N(x)_1) - x)\|_1 \quad (10)$$

where  $\|\cdot\|$  denotes the  $L_1$  norm, promoting sparse and robust reconstruction, especially useful for denoising subtle waveform features.

**Adversarial Loss:** The adversarial loss for the generator  $E$  with the discriminator  $C_1^X$  and  $C_2^X$  is given in Equation (11).

**Table 10**  
Class-wise metrics on the 12-lead ECG datasets.

Class	Precision (%)	Recall (%)	F1-score (%)	MCC	Balance accuracy (%)
Normal	97.5	98.9	98.2	0.95	98.2
MI (Myocardial Infarction)	89.4	90.1	89.5	0.85	89.8
ST/T Wave Changes (STTC)	91.3	88.2	89.6	0.87	89.6
Conduction Disturbances (CD)	90.2	85.3	87.6	0.82	87.7
Hypertrophy (HYP)	85.6	80.6	82.3	0.78	81.1

**Table 11**  
Distribution of ECG recordings in the 12-lead dataset.

Datasets	Normal	MI	STTC	CD	HYP	Total
Training (DS1)	8,000	5,500	4,700	3,200	2,600	24,000
Testing (DS2)	2,000	1,400	1,200	800	600	6,000
Total	10,000	6,900	5,900	4,000	3,200	30,000

$$L_E = L_E^g + E_{y \sim P_{data(y)}}[(C_2^X(E(y)_2) - 1)] \quad (11)$$

For generator  $N$  with discriminator  $C_1^Y$  and  $C_2^Y$  in Equation (12). where,

$$L_E = L_E^g + E_{y \sim P_{data(y)}}[(C_2^X(E(y)_2) - 1)^2] \quad (12)$$

For generator  $N$ , with a discriminator  $C_1^Y$  and  $C_2^Y$  in Equation (13).

$$L_F = L_F^g + E_{x \sim P_{data(x)}}[(C_2^Y(N(x)_2) - 1)] \quad (13)$$

where  $L_E^g$  and  $L_N^g$  denotes the guided loss, and the total loss is given in

Equation (14).

$$L_{E,N} = L_E + L_N \quad (14)$$

The discriminator loss is given in Equations (15) and (16).

$$L_{C_2^X} = \frac{1}{2} E_{y \sim P_{data(y)}}(C_2^X(E(y)_2) - 0) + \frac{1}{2} E_{x \sim P_{data(x)}}(C_2^X(x) - 1) \quad (15)$$

$$L_{C_2^Y} = \frac{1}{2} E_{x \sim P_{data(x)}}(C_2^Y(E(x)_2) - 0) + \frac{1}{2} E_{y \sim P_{data(y)}}(C_2^Y(y) - 1) \quad (16)$$

Discriminator total loss is given in Equation (17).

$$L_C = L_{C_2^X} + L_{C_2^Y} + L_{C_1^Y}^g + L_{C_1^X}^g \quad (17)$$

### 3.2.1. Artificial afterimage and color harmony algorithm to enhance classification accuracy

The AA technique imitates the continuing influence of characteristics through time whereas CH guarantees that the model treats its parameter space with a balanced and harmonious exploration. These two algorithms together guide the optimization steps of the Cycle-CMCHA-GAN

**Table 12**  
SHAP-based ECG feature contribution on 12-lead ECG dataset.

Feature	SHAP importance score	Interpretation
QRS Morphology Across Leads	0.380	Major contributor for multilead ventricular conduction analysis.
T-wave Abnormalities	0.320	Indicates ischemia, MI, electrolyte imbalance.
ST- segment deviations	0.270	Indicates ischemia, MI, electrolyte imbalance.
QTc interval	0.200	Shows ventricular repolarization duration across leads.
Lead-Specific voltage features	0.150	Reflect hypertrophy, axis deviation.
RR-interval	0.120	Captures rhythm regularity.

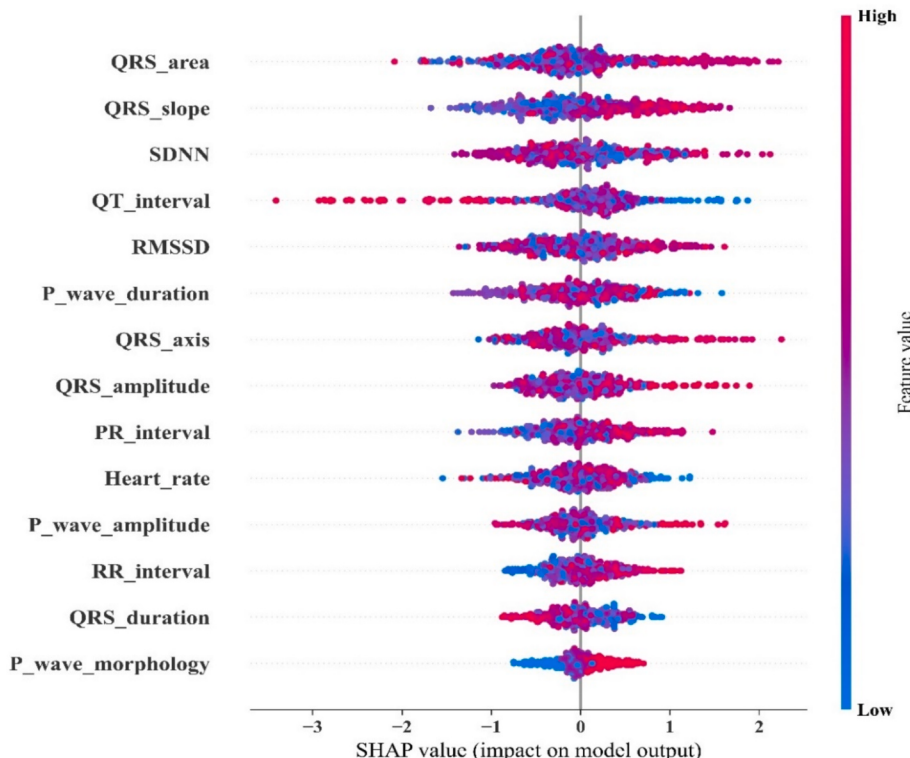


**Fig. 9.** SHAP summary plot for 12-lead ECG dataset.

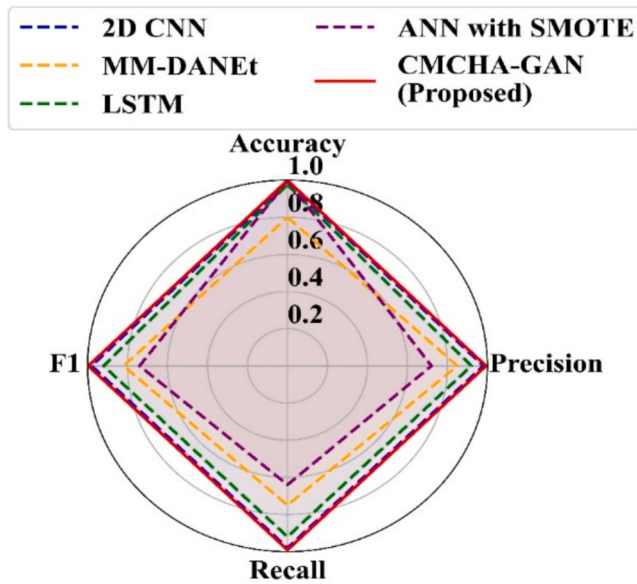


**Fig. 10.** Performance comparison on MIT-BIH Supra-ventricular Arrhythmia.

**Table 13**  
Class-wise Performance metrics on MIT-BIH Supra-ventricular Arrhythmia.

Class	Precision (%)	Recall (%)	F1-score (%)	MCC	Balance accuracy (%)
Normal	98.2	99.1	98.6	0.96	98.9
S/a	91.5	92.3	91.6	0.90	92.3
V	85.8	80.7	82.3	0.80	81.2
F	87.1	88.5	87.9	0.82	83.6
Q	88.3	83.1	83.2	0.87	85.3

**Table 14**  
Patient-level training and testing split with ECG beat distribution.

Datasets /Split	N/B	S/a	V	F	Q	Total
Training (DS1)	132,787	1,200	8,541	20	70	142,618
Testing (DS2)	32,000	830	300	15	43	33,188
Total	164,787	2,030	8,841	35	113	175,806

network through iterative refinements of candidate solutions [26,27]. The CH algorithm employs a method whereby it adjusts the parameter space in such a way as to maintain a balance throughout the optimization process, thus avoiding any feature being ignored or taking too much consideration over others. Conversely, the AA algorithm enhances the whole procedure by introducing a time factor and directing the network's search to those areas of hyperparameter space that result in more clinically useful ECG feature extraction.

**Table 5** shows the algorithm of AA and CH optimization. The initialization of key parameters includes population size, maximum iterations, decision variables, and color bounds, after which the candidate solutions are evaluated using a composite fitness function given in Equation (18).

$$F_i = \alpha \cdot L_{classification}(x_i) + \beta \cdot L_{harmony}(x_i) \quad (18)$$

where  $L_{classification}$  measures the classification loss and  $L_{harmony}$  penalizes violations of harmony constraints. This AA and CH optimization works in conjunction with the main Cycle-CMCHA-GAN loss components: cycle-consistency loss, dual-scale adversarial loss, and guided regularization. These collectively ensure faithful ECG signal translation and clinically meaningful feature preservation. The initial candidates subjected to alterations by visual-angle and afterimage effect are continuously adjusted by CH until they reach a point of convergence or

the set maximum number of iterations while keeping the global best solution noted down. The comprehensive description provided above makes it quite evident that perception-assisted adjustments, music correction and GAN-based losses all work hand-in-hand, thus granting methodological openness and reproducibility.

### 3.3. Explainable AI (SHAP)

The SHAP values are employed to improve explainability in the Cycle-CMCHA-GAN model for ECG classification [28]. The method not only identifies critical parts of the waveform but also increases transparency, instils confidence among clinicians, and facilitates precise decision-making in the real-time diagnosis of cardiac conditions. Cycle-CMCHA-GAN combines high-performance preprocessing, generative learning, and an artificial afterimage algorithm for increased accuracy and real-time detection. Explainability using SHAP enhances clinical trust, with performance.

## 4. Experimental analysis

Simulation experiments are performed with Python 3.10 and DL frameworks like TensorFlow and PyTorch to benchmark the effectiveness of the suggested Cycle-CMCHA-GAN approach for cardiac arrhythmia classification. Experiments are executed on a computer with an Intel Core i9-13900 K CPU, 64 GB RAM, and an NVIDIA RTX 4090 GPU (24 GB VRAM) for quick training and testing. **Table 6** explains about hyperparameter values of the proposed method.

### 4.1. Training details

The proposed Cycle-CMCHA-GAN and classifier were trained on an NVIDIA RTX 4090 GPU using Python 3.10, a batch of 64 samples, and 150 epochs. The AA optimizer used to guide CH with learning rate of 0.001, momentum 0.9, weight decay 1e-4, and exponential decay (0.96). The loss function combined cross-entropy, cycle-consistency, and adversarial losses with class-weighted regularization. Pre-processing involved the denoising of all ECG signals, normalization in the range of [-1, 1], and data augmentation by amplitude scaling, noise addition, and time warping. SMOTE was applied to balance the minority classes. Early stopping at patience = 10 and spectral normalization was employed to stabilize GAN training.

### 4.2. Performance comparison on the MIT-BIH dataset

The performance of the Cycle-CMCHA-GAN model is compared with other methods, such as ACoBi-LSTM [9], AlexNet [15], CNN-BiLSTM [10], BiLSTM [12], Fast Fourier Transform (FFT) + CNN + LSTM [11].

**Fig. 6** shows a performance comparison on the MIT-BIH dataset, where the higher accuracy of the Cycle-CMCHA-GAN is showcased. With a 99% on all evaluation metrics, it surpasses current methods such as ACoBi-LSTM, BiLSTM, and FFT + CNN-LSTM (98%), CNN-BiLSTM (97%), and AlexNet (96%). This proves the model's improved efficacy in cardiac arrhythmia classification. **Table 7** shows the class-wise metrics of the dataset.

The contribution of various ECG features, including QRS axis, RR variability, P-wave amplitude, QRS slope, QT interval, and PR interval, is shown in the SHAP summary plot represented in **Fig. 7**. It identifies the most influential features and how high or low values of these features shift outcomes, thus increasing interpretability and trust. **Table 8** shows the SHAP importance scores of key ECG features on the MIT-BIH dataset.

**Table 9** shows the class-wise distribution of ECG beats for the training and testing sets concerning five categories of AAMI EC57 heartbeat: Q, F, V, S, and N. Most of the beats are from class N, which represents the normal class.

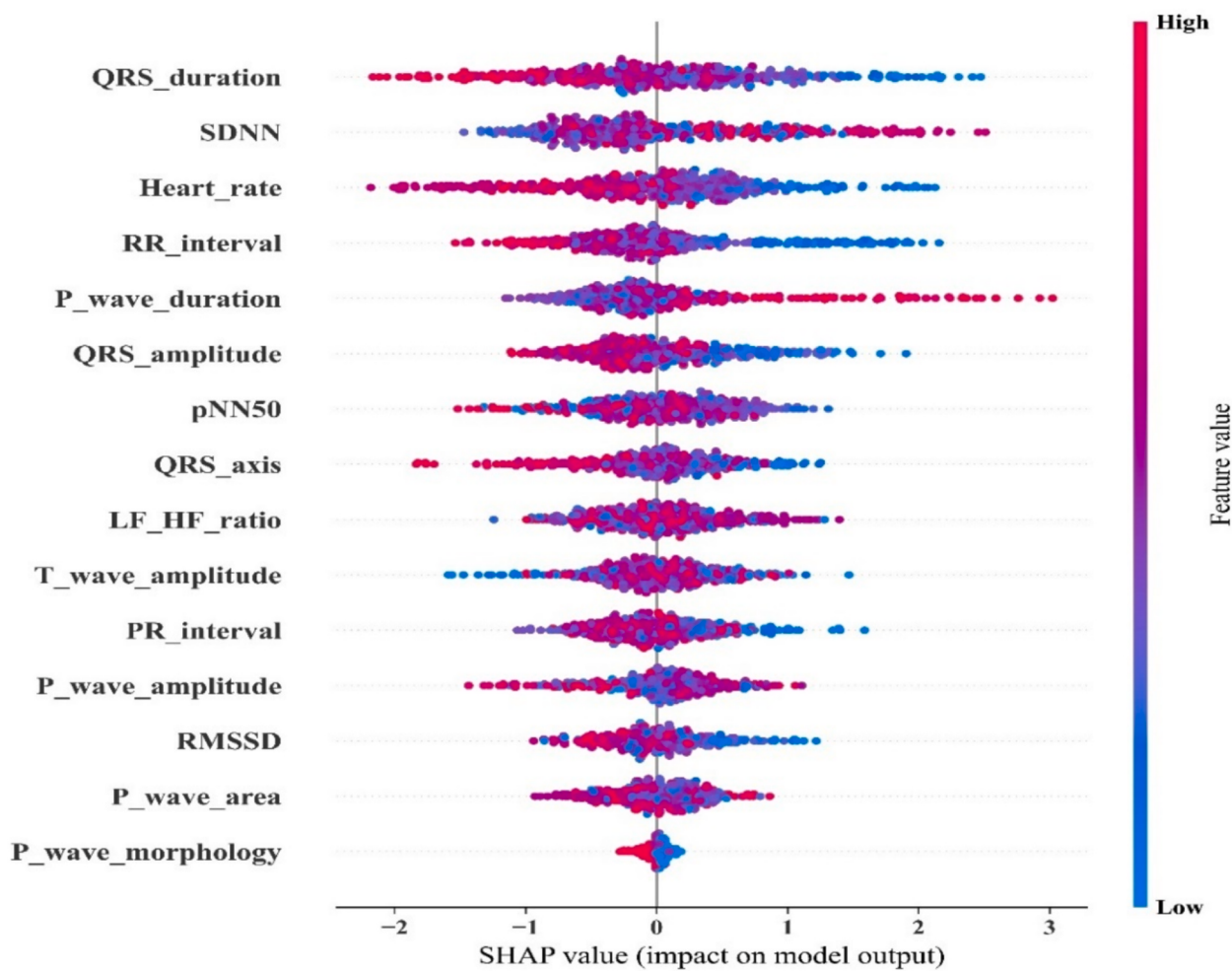


**Fig. 11.** SHAP summary plot on MIT-BIH Supra-ventricular Arrhythmia datasets.

**Table 15**  
SHAP-based ECG feature contribution on MIT-BIH Supra-ventricular Arrhythmia dataset.

Feature	SHAP importance score	Interpretation
P-wave Morphology	0.330	Most important for distinguishing supraventricular arrhythmias.
RR interval variability	0.300	Identifies irregular atrial rhythm patterns.
QRS complex	0.240	Supports detection of narrow/normal ventricular conduction.
T-wave shape	0.180	Indicates mild repolarization changes.
PQ interval	0.140	Reflects atrioventricular conduction timing.
Atrial activity energy	0.090	Captures atrial depolarization strength.

#### 4.3. Performance comparison on the 12-lead ECG dataset

The functionality of the Cycle-CMCHA-GAN method is compared with other existing methods, such as SRB-GCAB [13], MVKT [19], Multi-task Channel Attention network (MCA) [29], and Siamese CNN (SCNN) [30].

Fig. 8 depicts the performance of five models: Cycle-CMCHA-GAN, MVKT, MCA, SCNN, and SRB-GCAB. Of these, Cycle-CMCHA-GAN shows the best classification accuracy of almost 99% on all the evaluation measures. This indicates the strength of the proposed model in accurate and trustworthy cardiac arrhythmia classification based on

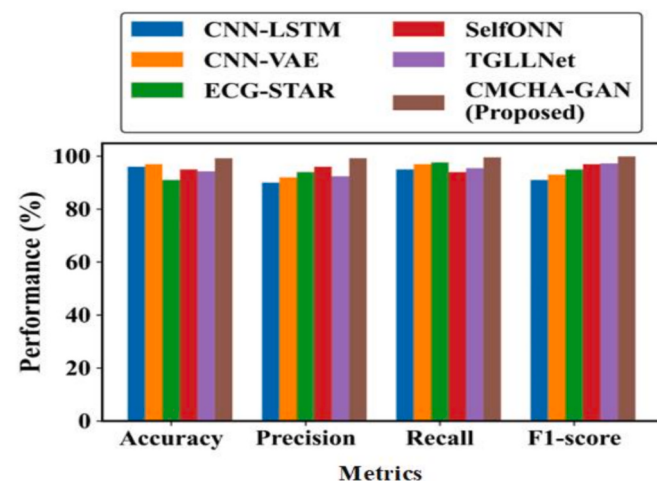


**Fig. 12.** Performance comparison on the PTB-XL datasets.

ECG signals. Table 10 shows the class-wise metrics on the 12-lead ECG datasets.

Table 11 illustrates the class-wise distribution of ECG recordings in the 12-lead dataset on five diagnostic classes: NORM, MI, STTC, CD, and HYP. The 24,000 samples for training and 6,000 for testing make the overall dataset consist of 30,000 records with balanced representation

**Table 16**

Class-wise performance metrics on the ptb-xl datasets.

Class	Precision (%)	Recall (%)	F1-score (%)	MCC	Balanced accuracy (%)
Normal	97.6	98.2	978.6	0.95	98.1
MI	90.2	91.3	90.3	0.86	91.2
STTC	91.4	89.7	90.3	0.88	89.8
CD	88.6	86.4	87.5	0.84	86.7
HYP	85.2	82.1	83.7	0.81	81.5

**Table 17**

Patient-level training and testing split with ECG beat distribution.

Dataset / Split	Normal	MI	STTC	CD	HYP	Total
Training (DS1)	14,500	5,500	4,700	3,200	2,600	30,500
Testing (DS2)	3,500	1,400	1,200	800	600	7,500
Total	18,000	6,900	5,900	4,000	3,200	38,000

for proper arrhythmia classification by DL models.

Fig. 9 indicates that every single ECG feature influence model prediction: QRS area, QT interval, RMSSD, PR interval, and RR interval. High and low feature values cause different shifts in SHAP scores, which show the most impactful parameters and improve model interpretability. Table 12 shows the SHAP importance scores of key ECG features on the 12-lead ECG dataset.

#### 4.4. Performance comparison on the MIT-BIH Supra-ventricular arrhythmia

The efficiency of the on MIT-BIH Supra-ventricular Arrhythmia is compared with other existing methods such as 2DCNN [20], Artificial Neural Network with Synthetic Minority Over-sampling Technique (ANN with SMOTE), MM-DANet [21], and LSTM [14].

Fig. 10 shows the comparison of performance on the MIT-BIH Supraventricular Arrhythmia dataset. The best accuracy of 0.99 is obtained

by the proposed Cycle-CMCHA-GAN, followed by all other models. Whereas 2D CNN and LSTM exhibit moderate performance. ANN with SMOTE is the weakest among all the evaluation metrics, indicating its poor classification ability. Table 13 explains the class-wise performance metrics on the MIT-BIH Supra-ventricular Arrhythmia.

Table 14 shows the distribution of ECG beats over the training and test datasets. The majority are normal beats (N/B), then ventricular (V) and S/a beats are infrequent. It consists of 175,806 beats in total, enabling strong DL-based arrhythmia classification and generalization across beat types.

Fig. 11 explains that the SHAP plot indicates that ECG features such as QRS duration, RR interval, SDNN, pNN50, PR interval, and T-wave amplitude impact the model's predictions. High and low feature values push SHAP scores, revealing which parameters have the most impact and improving model interpretability. Table 15 shows the SHAP importance scores of key ECG features.

#### 4.5. Performance comparison on the PTB-XL datasets

The performance of the proposed method compared with existing approaches: CNN-LSTM [22], SelfONN [31], CNN-VAE [32], Spatio-

**Table 18**  
SHAP-based ECG feature contribution on PTB-XL dataset.

Feature	SHAP importance score	Interpretation
ST-Segment	0.360	Most important for detecting MI and ST-T abnormalities.
T-wave Features	0.310	Captures repolarization abnormalities in ischemic patterns.
QRS complex	0.260	Indicates conduction abnormalities (LBBB/RBBB).
QT interval	0.190	Important for prolonged QT and ventricular repolarization issues.
RR interval	0.160	Represents heart rate variability.
P-wave shape	0.110	Reflects atrial activity and enlargement detection.

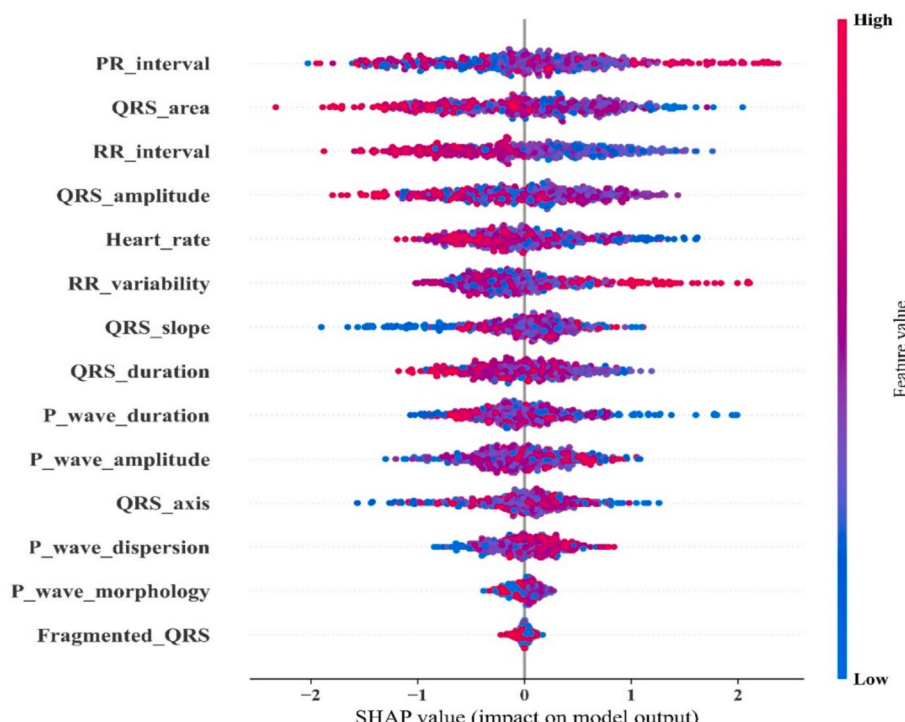
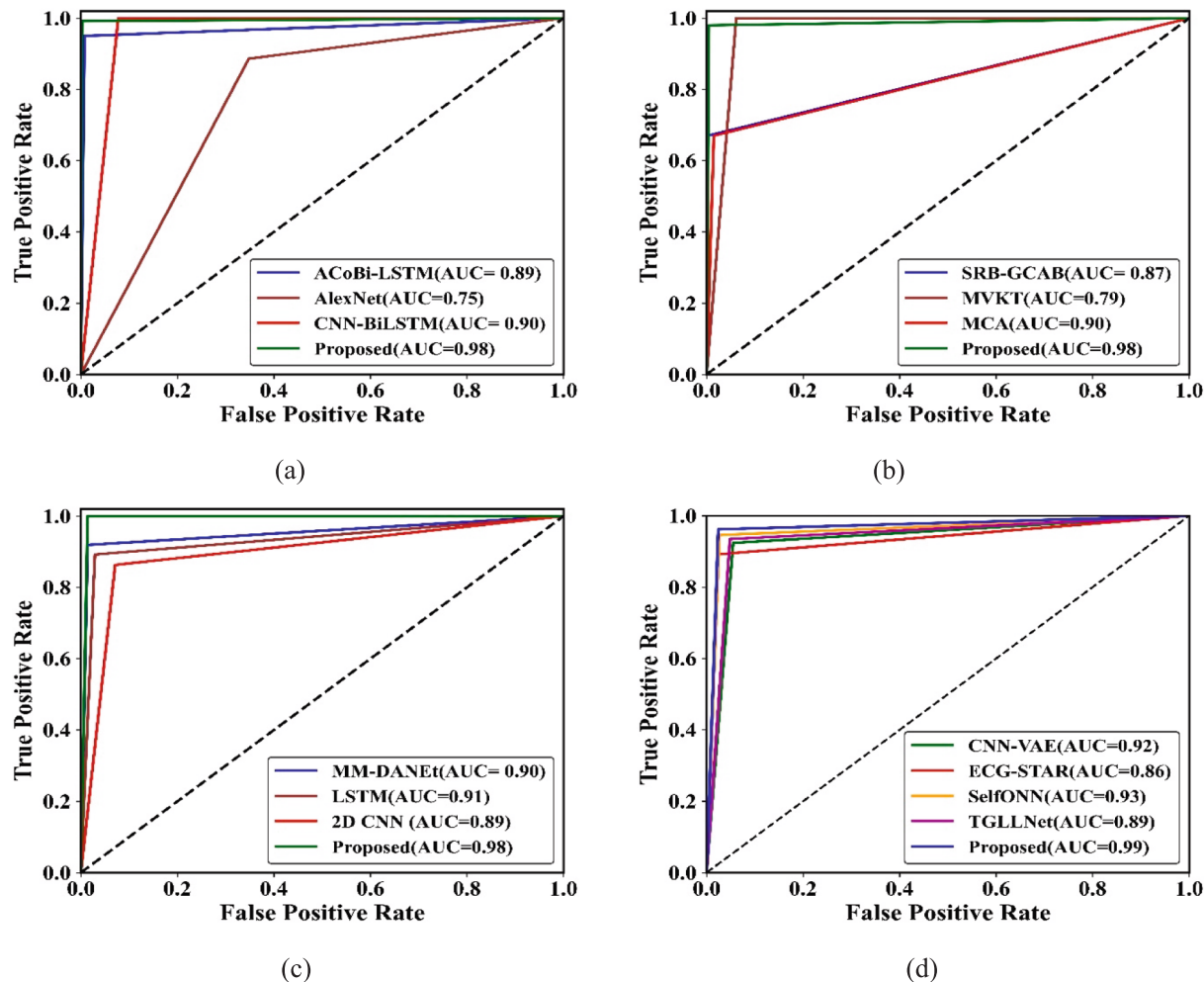


Fig. 13. SHAP summary plot on PTB-XL dataset.



**Fig. 14.** ROC curve of (a) MIT-BIH Arrhythmia, (b) MIT-BIH Supra-ventricular Arrhythmia, (c) 12-lead ECG dataset and (d)PTB-XL datasets.

Temporal Attention Residual Networks (ECG-STAR) [33], and Task-Guided Lead Correlations (TGLLNet) [34]. It outperformed these models in ECG classification and feature extraction.

Fig. 12 demonstrates the effectiveness of the proposed CMCHA-GAN, showing its capability of significantly enhancing the classification of ECG in contrast to other existing methods. Table 16 shows the class-wise metrics on the PTB-XL datasets.

Table 17 shows that the comprises five cardiac diseases, along with distinct training and testing splits. Normal beats constitute the majority of the samples, whereas the other classes (i.e., MI, STTC, CD, and HYP) are very evenly represented, which helps to guarantee trustworthy model training and evaluation.

Fig. 13 demonstrates how different features from an ECG affect the model output. Examples of such features are the PR interval and QR area with differing SHAP values, thereby having different influences on the model. Table 18 shows the SHAP importance scores of key ECG features on the PTB-XL dataset.

#### 4.6. ROC curve analysis

Fig. 14 (a-d) shows the ROC curves with respect to different models comparing performances on different ECG datasets. This indicates that the proposed model outperformed others in terms of higher AUC markers for effectiveness in arrhythmia detection

#### 4.7. Confusion matrix analysis

Fig. 15 shows the confusion matrix for the proposed method on the different ECG datasets mentioned above. The matrices signify the performance of the model, showing the correct and misclassified labels in each category, with very high accuracies across datasets.

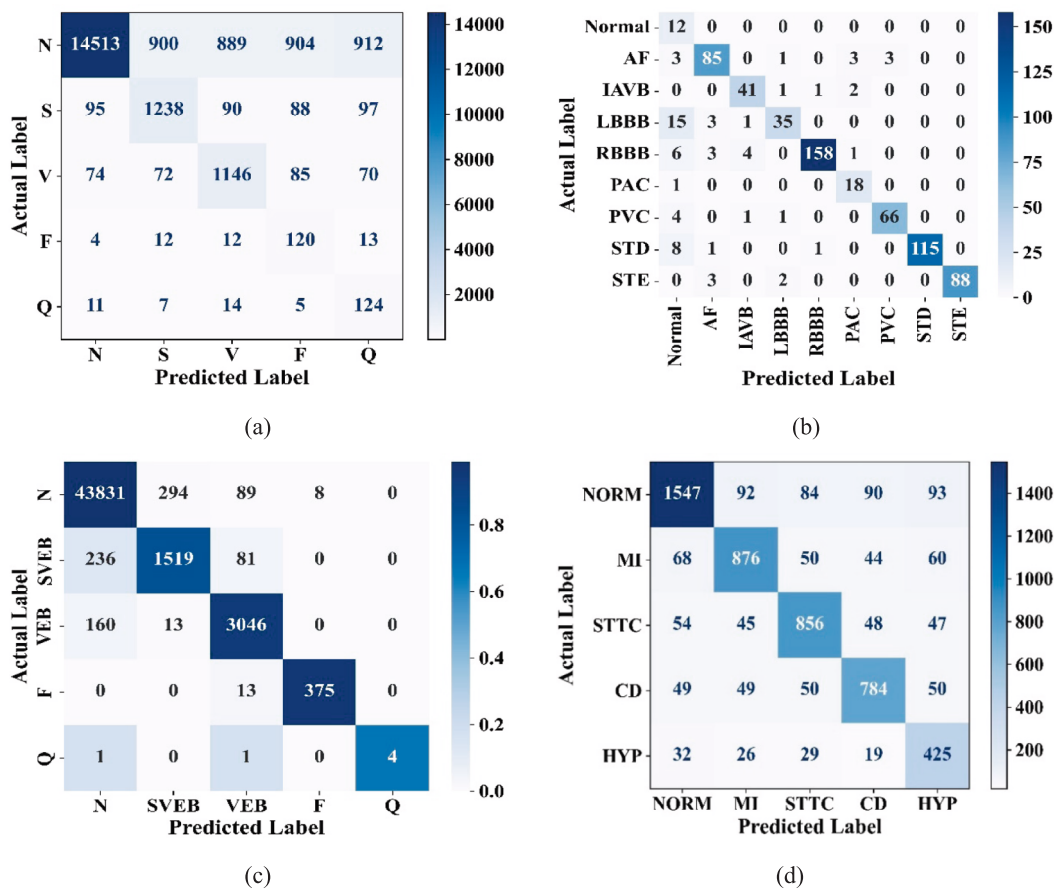
#### 4.8. Training curve of the proposed method

Fig. 16(a-d) illustrates the training curves of the proposed method on four disparate datasets. Demonstrating how the proposed method's performance is influenced by the training ability to learn across the datasets and generalize.

#### 4.9. Model complexity and performance comparison

The differences in computational efficiency are revealed as the model complexity and performance connotate a comparative analysis of parameters, FLOPs, and accuracy, demonstrating the superior balance attained by the proposed method.

Table 19 provides a comparison between the statistical and performance indicators of the proposed Cycle-CMCHA-GAN model against existing ECG classification methods in wide use. Therefore, the proposed model yields the lowest entropy of 0.71, indicating the least prediction uncertainty, and the highest specificity of 98.7%, thus showing good ability in distinguishing normal from abnormal beats. Moreover, with an average accuracy of 97%, the proposed technique distinctly outperforms



**Fig. 15.** Confusion matrix on (a) MIT-BIH Arrhythmia, (b) MIT-BIH Supra-ventricular Arrhythmia, (c) 12-lead ECG dataset and (e)PTB-XL datasets.

other conventional architectures comprising CNN-LSTM, CNN-BiLSTM, and AlexNet, thus confirming that it is highly reliable and robust for ECG classification. Table 20 shows the computational cost of the proposed method.

Fig. 17 illustrates the computational expenses of various models. The presented model has the least computational cost, significantly lower than LSTM [8], ACoBi [5], and BiLSTM [10].

#### 4.10. Cross-validation

Table 21 shows the 5-fold cross-validation results of the four external datasets, showing consistently high among the folds, accompanied by very small standard deviations, confirming its robustness and reliability for classification.

Table 22 shows that the proposed model is tested on various outside ECG datasets and continues to perform well in every case, which is a sign of strong generalization and a confirmation that the results are not a consequence of overfitting the training data.

#### 4.11. Statistical configuration of ECG datasets

The statistical setup defines critical properties of the ECG datasets employed. It involves overall samples, mean signal length, sampling frequency, number of channels/leads, arrhythmia categories, and types of annotations.

Table 23 explains the statistical configuration of ECG datasets. It consolidates significant features of the MIT-BIH, 12-lead ECG, and Supraventricular datasets in terms of sample size, signal length, sampling frequency, number of leads, class types, and annotation style. It highlights the factors of dataset structure, class distribution, and annotation detail that are crucial for model training, testing, and clinical

application. Table 24 shows the statistical comparisons between the proposed Cycle-CMCHA-GAN and CNN-LSTM.

#### 4.12. Ablation study

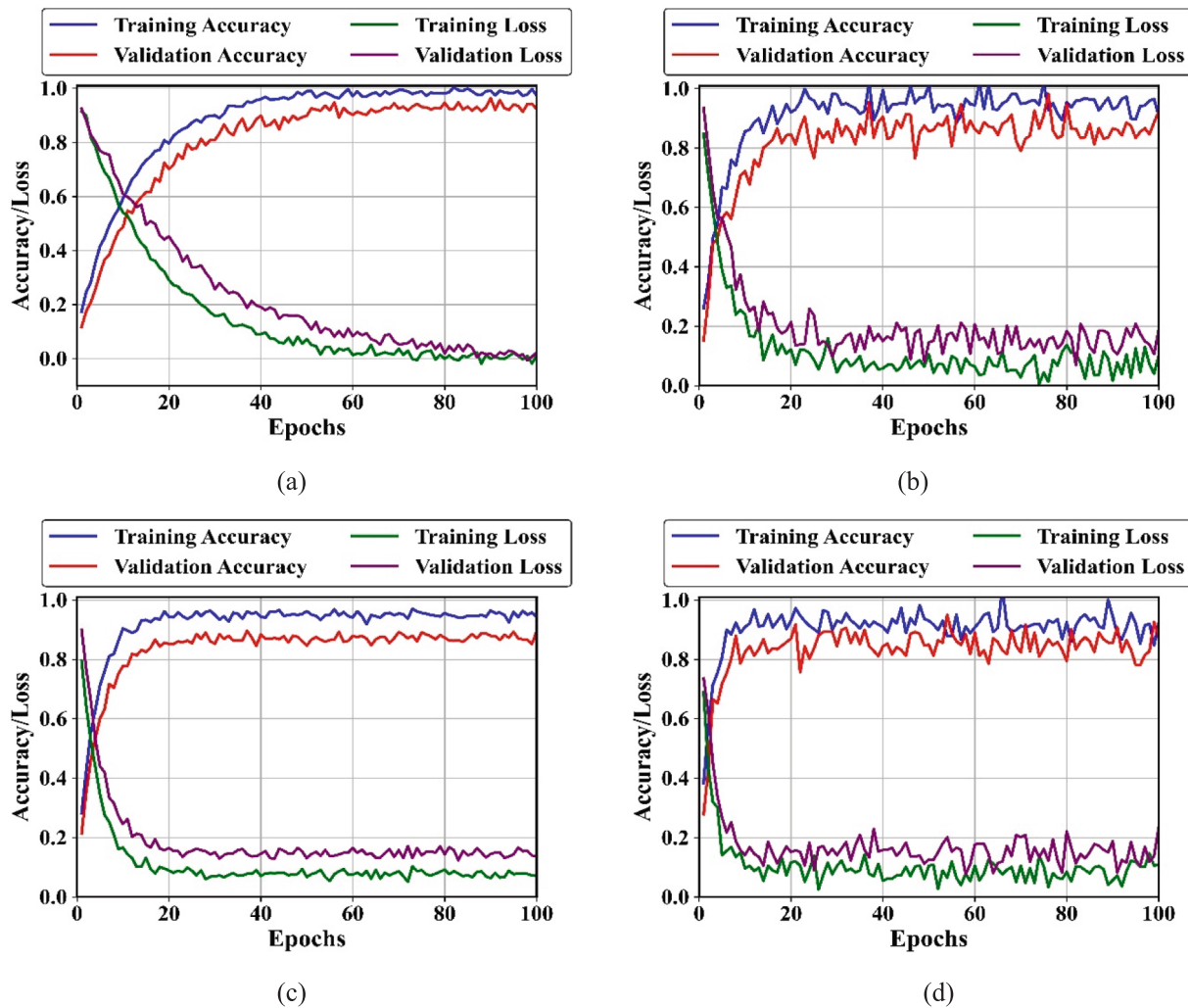
By systematically removing elements like the AA module, CH encoding, or momentum convolution, the analysis demonstrates an impact on classification performance, validating their necessity for optimal ECG arrhythmia detection.

Table 25 illustrates that every module helps the functionality of the suggested ECG classification model. Omitting the momentum-based generator, dual discriminators, colour harmony loss, or afterimage augmentation lowers the performance level.

Table 26 shows an ablation study of different regularization methods, such as Dropout, L2 Weight Decay, Batch Normalization, and Early Stopping. The results indicate that correct regularization brings the effect of stabilizing training, reducing overfitting.

#### 4.13. Discussion

The findings from the experiment show that the proposed model is able to consistently outperform the existing techniques over various ECG datasets. The model offers very high classification performance with an accuracy rate of up to 99.88% on the 12-lead ECG and PTB-XL datasets, thereby able to perfectly capture the complex temporal and spatial dependencies in the ECG signals. SHAP analysis reveals the important ECG features that are responsible for the predictions, making the model more interpretable. The cross-validation results and training curves indicate a stable convergence with no overfitting. The confusion matrices and ROC curves show the model's strong discriminative power across all the classes. The ablation studies on regularization and hyperparameters also



**Fig. 16.** Training curves on (a) MIT-BIH Arrhythmia, (b) MIT-BIH Supra-ventricular Arrhythmia, (c) 12-lead ECG dataset and (d)PTB-XL datasets.

**Table 19**  
Statistical and Performance Measures of the ECG Classification Model.

Metrics	Proposed Cycle-CMCHA-GAN	CNN-LSTM [11]	CNN-BiLSTM [10]	AlexNet [15]
Kurtosis	3.21	2.87	3.05	2.76
Specificity (%)	98.7	96.4	95.7	94.8
Entropy	0.71	0.89	0.93	0.98
Mean accuracy (%)	97	95.2	94.7	93.8

**Table 20**  
Comparison of Parameters, FLOPS, and Accuracy Across Models.

Method	Params (M)	FLOPS (G)	Accuracy (%)
LSTM [11]	8.4	3.5	98.67
CNN-BiLSTM [10]	11.3	2.7	97.67
MVKT [19]	7.5	7.1	98.16
AlexNet [15]	6.3	4.34	98.87
Proposed	5.0	2.1	99.93

confirm the model's generalization. The statistical tests against CNN-LSTM also indicate a significant gain ( $p < 0.0001$ ). In general, the model displays excellent consistency and reproducibility in performance over different datasets.

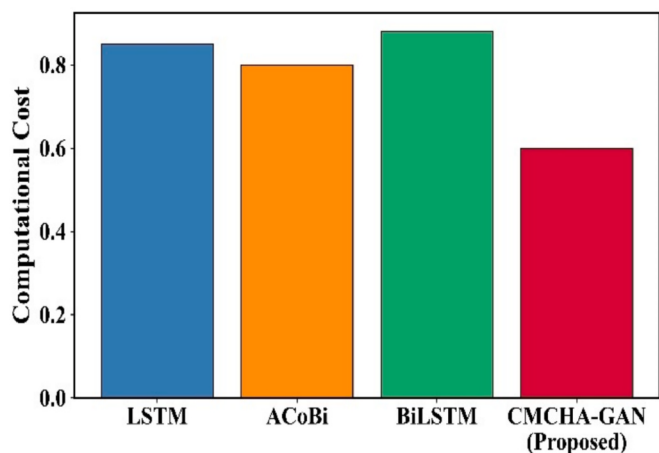


**Fig. 17.** Computational cost analysis.

#### 4.14. Limitations

The limitations of the research include the lack of clinical and multicenter validations, which restrict the assessment of the model's robustness to diverse patient populations and different acquisition conditions. Moreover, the real-world applicability has not been

**Table 21**  
Cross-validation of the proposed method.

Fold	Accuracy (%)	F1-score (%)	Precision (%)	Recall (%)
Fold 1	99.6 ± 0.2	99.5 ± 0.2	99.7 ± 0.1	99.4 ± 0.3
Fold 2	99.5 ± 0.3		99.6 ± 0.1	99.5 ± 0.2
		99.4 ± 0.2		
Fold 3	99.7 ± 0.1		99.8 ± 0.2	99.6 ± 0.1
		99.6 ± 0.1		
Fold 4	99.6 ± 0.2	99.5 ± 0.2	99.7 ± 0.2	99.5 ± 0.2
Fold 5	99.5 ± 0.2	99.4 ± 0.1	99.6 ± 0.2	99.4 ± 0.2
Mean ± SD	99.58 ± 0.08	99.48 ± 0.07	99.68 ± 0.06	99.48 ± 0.08

**Table 22**  
Performance on External ECG Datasets.

Datasets	Accuracy (%)	Precision (%)	Recall (%)	F1-Score (%)
MIT-BIH Arrhythmia	99.87	99.67	99.78	99.67
MIT-BIH Supraventricular Arrhythmia	99.88	99.78	99.78	99.75
12-lead ECG	99.88	99.87	99.86	99.86
PTB-XL ECG	99.88	99.78	99.69	99.78
Shaoxing & Ningbo Hospital (external datasets) [35]	98.78	98.78	98.72	98.34
INCART 12-lead (external datasets) [36]	98.67	98.67	98.45	98.12

validated yet, and more experimental testing is required to verify the generalization the reliability and effectiveness of the Cycle-CMCHA-GAN framework in clinical practice.

## 5. Conclusion

A Cycle-CMCHA-GAN, an interpretable DL system, is introduced for the ECG signals-based automatic classification of cardiac arrhythmias. The model handles problems like signal variability, low-amplitude patterns, and inter-class similarity through advanced denoising, wavelet feature extraction, and artificial afterimage optimization. The momentum-based generator and dual discriminators model simultaneously extract global and local heartbeat features, and the AA algorithm improves convergence and hyperparameter tuning. The SHAP analysis brings forth the explainability aspect by pinpointing the influential ECG features, hence augmenting the model's interpretability. The model demonstrates excellent generalizability on diverse datasets. Nevertheless, it is still under experimental conditions for clinical use due to the need for thorough multicenter validation. Although this model has very strong generalizability, the clinical application remains very

**Table 25**  
Ablation experiment on key components.

Model configuration	Accuracy (%)	Precision (%)	Recall (%)	F1 score (%)	AUC
With all components (Full Proposed Model)	99.2	99.7	99.45	99.5	0.98
Without a Momentum-based Generator	97	97	98	97	0.96
Without the denoising process	95	95	95	95	95
Without afterimage and color harmony optimization	96	96	96	96	96

limited since it is not a multicenter-validated model. Future work will be directed toward the implementation of secure federated learning, which will allow for decentralized ECG analysis across different institutions while preserving patient privacy. In parallel, an investigation will be performed on edge-based deployment to support real-time monitoring in wearable devices and IoT environments. Furthermore, integration of multimodal physiological signals-PPG, heart sounds, and respiration-will be pursued to enhance model robustness by improving the detection of rare and complex arrhythmias and allowing more accurate patient-specific classification.

## CRediT authorship contribution statement

**P. Kavitha:** Validation, Conceptualization. **L. Shakkeera:** Writing – review & editing, Writing – original draft.

**Table 26**  
Ablation Study of the Proposed Method with Regularization Methods.

Regularization Method	Value	Accuracy (%)	Precision (%)	F1-score (%)	Recall (%)
Dropout	0.3	99.2	99.7	99.45	99.5
L2 Weight Decay	0.2	98.4	97.12	97.32	98.34
	0.001	99.2	99.7	99.45	99.5
	0.01	98.4	97.1	96.5	96.5
Batch Normalization	With BN	99.2	99.7	99.45	99.5
	Without BN	97.3	97.5	96.4	96.5
Early Stopping	Patience = 10	99.2	99.7	99.45	99.5
	Patience = 20	98.4	97.6	97.78	96.5

**Table 23**  
Statistical Configuration of ECG Datasets.

Dataset	Total samples	Signal length	Sampling rate	Lead/channel	classes	Annotation type
MIT-BIH Arrhythmia	99,772	30 min/record (avg)	360	2 (MLII, V1/II)	N, S, V, F, Q	Beat-level annotations (AAMI)
12-Lead ECG	30,000	10 s	500	12	NORM, MI, STTC, CD, HYP	Diagnostic-level annotation
MIT-BIH Supra-ventricular Arrhythmia	175,806	30 min/record (avg)	128	2	N/B, S/a, V, F, Q	Beat-level annotations (AAMI)

**Table 24**  
Statistical Significance Analysis Comparing Cycle-CMCHA-GAN with CNN-LSTM Across Multiple ECG Datasets.

Test type	Dataset	Compared methods	Accuracy (Mean ± SD) [95% CI]	t-Statistic	p-Value	Significance (95% CI)
Paired t-Test	MIT-BIH Arrhythmia	Cycle-CMCHA-GAN vs CNN-LSTM	99.87 ± 0.02 vs 97.65 ± 0.10	t (19) = 5.87	<0.0001	Significant
Paired t-Test	MIT-BIH Supraventricular	Cycle-CMCHA-GAN vs CNN-LSTM	99.88 ± 0.02 vs 97.80 ± 0.09	t (19) = 6.05	<0.0001	Significant
Paired t-Test	PTB-XL ECG	Cycle-CMCHA-GAN vs CNN-LSTM	99.88 ± 0.02 vs 96.90 ± 0.12	t (19) = 6.40	<0.0001	Significant
Paired t-Test	12-lead ECG	Cycle-CMCHA-GAN vs CNN-LSTM	99.88 ± 0.02 vs 97.50 ± 0.08	t (19) = 6.15	<0.0001	Significant

## Funding

This research did not receive any specific grant from funding agencies in the public, commercial, or not-for-profit sectors.

## Declaration of competing interest

The authors declare that they have no known competing financial interests or personal relationships that could have appeared to influence the work reported in this paper.

## Acknowledgement

None

## Data availability

No data was used for the research described in the article.

## References

- [1] M.U. Zahid, S. Kiranyaz, M. Gabbouj, Global ECG classification by self-operational neural networks with feature injection, *IEEE Trans. Biomed. Eng.* 70 (2022) 205–215, <https://doi.org/10.1109/tbme.2022.3187874>.
- [2] S. Yang, C. Lian, Z. Zeng, B. Xu, J. Zang, Z. Zhang, A multi-view multi-scale neural network for multi-label ECG classification, *IEEE Trans. Emerging Top. Comput. Intell.* 7 (2023) 648–660, <https://doi.org/10.1109/teci.2023.3235374>.
- [3] D. Al-Shammary, M.N. Kadhim, A.M. Mahdi, A. Ibaida, K. Ahmed, Efficient ECG classification based on Chi-square distance for arrhythmia detection, *J. Electron. Sci. Technol.* 22 (2024) 100249, <https://doi.org/10.1016/j.jnest.2024.100249>.
- [4] A. Soman, R. Sarath, Optimization-enabled deep convolutional neural network with multiple features for cardiac arrhythmia classification using ECG Signals, *Biomed. Signal Process. Control* 92 (2024) 105964, <https://doi.org/10.1016/j.bspc.2024.105964>.
- [5] W. Ji, D. Zhu, ECG classification exercise health analysis algorithm based on GRU and convolutional neural network, *IEEE Access* 12 (2024) 59842–59850, <https://doi.org/10.1109/access.2024.3392965>.
- [6] S. Sattar, R. Mumtaz, M. Qadir, S. Mumtaz, M.A. Khan, T. De Waele, et al., Cardiac arrhythmia classification using advanced deep learning techniques on digitized ECG datasets, *Sensors* 24 (2024) 2484, <https://doi.org/10.3390/s24082484>.
- [7] J. Shao, S. Geng, Z. Fu, W. Xu, T. Liu, S. Hong, Cardiodefense: defending against adversarial attack in ECG classification with adversarial distillation training, *Biomed. Signal Process. Control* 91 (2024) 105922, <https://doi.org/10.1016/j.bspc.2023.105922>.
- [8] A. Pal, H.M. Rai, S. Agarwal, N. Agarwal, Advanced noise-resistant electrocardiography classification using hybrid wavelet-median denoising and a convolutional neural network, *Sensors* 24 (2024) 7033, <https://doi.org/10.3390/s24217033>.
- [9] S. Lamba, S. Kumar, M. Diwakar, Fadlec: Feature extraction and arrhythmia classification using Deep Learning from electrocardiograph signals, *Discover Artificial Intelligence.* 5 (2025) 1–7, <https://doi.org/10.1007/s44163-025-00290-0>.
- [10] S. Bhatia, S.K. Pandey, A. Kumar, A. Alshuhail, Classification of electrocardiogram signals based on hybrid deep learning models, *Sustainability* 14 (2022) 16572, <https://doi.org/10.3390/su142416572>.
- [11] A. Eleyan, E. Alboghaibah, Electrocardiogram signals classification using deep-learning-based incorporated convolutional neural network and long short-term memory framework, *Computers* 13 (2024) 55, <https://doi.org/10.3390/computers13020055>.
- [12] J. Lim, D. Han, M.P. Shirazi Nejad, K.H. Chon, ECG classification via integration of adaptive beat segmentation and relative heart rate with Deep Learning Networks, *Comput. Biol. Med.* 181 (2024) 109062, <https://doi.org/10.1016/j.combiomed.2024.109062>.
- [13] H.K. Kim, M.H. Sunwoo, An automated cardiac arrhythmia classification network for 45 arrhythmia classes using 12-lead electrocardiogram, *IEEE Access* 12 (2024) 44527–44538, <https://doi.org/10.1109/access.2024.3380892>.
- [14] R. de Guerra, C.K. Yamaguchi, S.F. Stefenon, L. dos Coelho, V.C. Mariani, Deep Learning Approach for Automatic Heartbeat Classification, *Sensors* 25 (2025) 1400, <https://doi.org/10.3390/s25051400>.
- [15] A. Rahman, R.N. Asif, K. Sultan, S.A. Alsaif, S. Abbas, M.A. Khan, et al., ECG classification for detecting ECG arrhythmia empowered with deep learning approaches, *Comput. Intell. Neurosci.* 2022 (2022) 1–12, <https://doi.org/10.1155/2022/6852845>.
- [16] Y. Xia, Y. Xu, P. Chen, J. Zhang, Y. Zhang, Generative adversarial network with transformer generator for boosting ECG classification, *Biomed. Signal Process. Control* 80 (2023) 104276, <https://doi.org/10.1016/j.bspc.2022.104276>.
- [17] J. Zarean, A. Tajally, R. Tavakkoli-Moghaddam, R. Kia, Robust electroencephalogram-based biometric identification against gan-generated artificial signals using a novel end-to-end attention-based CNN-LSTM Neural Network, *Clust. Comput.* 28 (2025) 168, <https://doi.org/10.1007/s10586-024-04921-6>.
- [18] S. Haseena Beegum, R. Manju, Gan-based novel feature selection approach with hybrid deep learning for heartbeat classification from ECG Signal, *Comput. Biol. Chem.* 120 (2026) 108704, <https://doi.org/10.1016/j.combiolchem.2025.108704>.
- [19] Y. Qin, L. Sun, H. Chen, W. Yang, W.-Q. Zhang, J. Fei, et al., MVKT-ECG: Efficient single-lead ECG classification for multi-label arrhythmia by multi-view knowledge transferring, *Comput. Biol. Med.* 166 (2023) 107503, <https://doi.org/10.1016/j.combiomed.2023.107503>.
- [20] H. Ullah, M.B. Bin Heyat, F. Akhtar, A.Y. Sumbul, M.S. Muaad Islam, et al., An end-to-end cardiac arrhythmia recognition method with an effective DenseNet model on imbalanced datasets using ECG Signal, *Comput. Intell. Neurosci.* (2022) 1–23, <https://doi.org/10.1155/2022/9475162>.
- [21] Z. Xu, M. Zang, T. Liu, Z. Wang, S. Zhou, C. Liu, et al., Multimodality data augmentation network for Arrhythmia Classification, *Int. J. Intell. Syst.* 2024 (2024), <https://doi.org/10.1155/2024/9954821>.
- [22] A.E. Atwa, E.-S. Atlam, A. Ahmed, M.A. Atwa, E.M. Abdelrahim, A.I. Siam, Interpretable deep learning models for arrhythmia classification based on ECG signals using PTB-X Dataset, *Diagnostics* 15 (2025) 1950, <https://doi.org/10.3390/diagnostics15151950>.
- [23] D. Pal, S. Mukhopadhyay, R. Gupta, ENSEMBLED data augmentation model for simplified cardiac arrhythmia detection under limited minority class data, *IEEE Trans. Instrum. Meas.* 73 (2024) 1–9, <https://doi.org/10.1109/tim.2024.3460887>.
- [24] G. Gao, H. Lai, Z. Jia, Unsupervised image dedusting via a cycle-consistent generative adversarial network, *Remote Sens. (Basel)* 15 (2023) 1311, <https://doi.org/10.3390/rs15051311>.
- [25] R. Rahimilarki, Z. Gao, N. Jin, A. Zhang, Convolutional Neural Network Fault classification based on time-series analysis for Benchmark Wind Turbine Machine, *Renew. Energy* 185 (2022) 916–931, <https://doi.org/10.1016/j.renene.2021.12.056>.
- [26] M. Demir, Artificial afterimage algorithm: a new bio-inspired metaheuristic algorithm and its clustering application, *Appl. Sci.* 15 (2025) 1359, <https://doi.org/10.3390/app15031359>.
- [27] P.S. Senthil, selvi A. Senthil, T. Kumaragurubaran, S. Dhanasekaran, Self-attention-based generative adversarial network optimized with color harmony algorithm for Brain Tumor Classification, *Electromagnetic Biology and Medicine*. 43 (2024) 31–45. doi:10.1080/15368378.2024.2312363.
- [28] D. Gaspar, P. Silva, C. Silva, Explainable AI for intrusion detection systems: Lime and shap applicability on Multi-Layer Perceptron, *IEEE Access* 12 (2024) 30164–30175, <https://doi.org/10.1109/access.2024.3368377>.
- [29] W. Pan, Y. An, Y. Guan, J. Wang, MCA-Net: a multi-task channel attention network for myocardial infarction detection and location using 12-lead egs, *Comput. Biol. Med.* 150 (2022) 106199, <https://doi.org/10.1016/j.combiomed.2022.106199>.
- [30] M.E. Vasconcellos, B.G. Ferreira, J.S. Leandro, B.F. Neto, F.R. Cordeiro, I.A. Cestari, et al., Siamese convolutional neural network for Heartbeat Classification using limited 12-lead ECG datasets, *IEEE Access* 11 (2023) 5365–5376, <https://doi.org/10.1109/access.2023.3236189>.
- [31] K. Qin, W. Huang, T. Zhang, H. Zhang, X. Cheng, A lightweight SELFONN model for general ECG classification with pretraining, *Biomed. Signal Process. Control* 89 (2024) 105780, <https://doi.org/10.1016/j.bspc.2023.105780>.
- [32] I.J. Selvam, M. Madhavan, S.K. Kumarasamy, Detection and classification of electrocardiography using hybrid deep learning models, *Hellenic J. Cardiol.* 81 (2025) 75–84, <https://doi.org/10.1016/j.hjc.2024.08.011>.
- [33] C.-L. Liu, B. Xiao, C.-F. Tsai, ECG-Star: Spatio-temporal attention residual networks for multi-label ECG abnormality classification, *Inf. Sci.* 717 (2025) 122273, <https://doi.org/10.1016/j.ins.2025.122273>.
- [34] X. Yuan, W. Wang, J. Chen, K. Fang, A. Kashif Bashir, T. Mondal, et al., Enhancing multilabel ECG classification via task-guided lead correlations in internet of medical things, *IEEE Internet Things J.* 12 (2025) 20544–20555, <https://doi.org/10.1109/jiot.2025.3544224>.
- [35] T. Leinonen, D. Wong, A. Vasankari, A. Wahab, R. Nadarajah, M. Kaisti, et al., Empirical investigation of multi-source cross-validation in clinical ECG classification, *Comput. Biol. Med.* 183 (2024) 109271, <https://doi.org/10.1016/j.combiomed.2024.109271>.
- [36] D.H. Elsheikhy, A.S. Hassan, N.M. Yhiea, A.M. Fareed, E.A. Rashed, Lightweight deep learning architecture for multi-lead ECG arrhythmia detection, *Sensors* 25 (2025) 5542, <https://doi.org/10.3390/s25175542>.